fluids

MDPI

Article

Research on the Influence of Channel Bending on Control Rod Drop

Siyu Zou *, Chang'e Wu, Yangyang Tang, Qifeng Lv, Yue Ma and Jinghua Tang

China Nuclear Power Technology Research Institute Co., Ltd., Shenzhen 518031, China; cewu@mail.ustc.edu.cn (C.W.); tangyuanyuan07@163.com (Y.T.); phlippelv@126.com (Q.L.); mayue199909@163.com (Y.M.); tjh016@163.com (J.T.)
* Correspondence: zousiyude@163.com

Abstract

Research on the effect of channel bending on control rod drop is crucial; this paper employs FLUENT dynamic mesh technology to study the drop behavior of a control rod in a simplified control rod channel after bending deformation. It compares the differences in rod drop under different fluid media and various bent channel geometries (straight channel, C-shaped bent channel, S-shaped bent channel), and analyzes the variation patterns of rod drop time, velocity, static pressure, dynamic pressure, and flow field. The results show that under C-shaped and S-shaped bends, the changes in the flow field when the control rod descends without contacting the channel have no effect on the rod drop time.

Keywords: control rod drop; CFD; dynamic mesh; channel bending

1. Introduction

The smooth drop of the control rod is critical for ensuring the safe shutdown of the reactor, and the rod drop time significantly affects core safety. The primary causes of fuel assembly bending are thermal expansion, irradiation, and creep of fuel rods [1]. During in-core operation, fuel assemblies may undergo bending deformations, with the main bending shapes being "C-shaped bending", "S-shaped bending", and "W-shaped bending" [2]. Excessive bending of fuel assemblies increases the core power peaking factor and quadrant power tilt, reducing the thermal margin of the core. In 2000, Unit 2 of the Ringhals nuclear power plant in Sweden experienced quadrant power tilt caused by assembly bending, which subsequently restricted its ability to perform load following [3]. Excessive bending can also lead to grid-to-grid fretting wear, potentially causing fuel assembly failure [4]. In addition, excessive bending of fuel assemblies may cause difficulties in fuel loading and unloading, as well as preventing the control rod from being fully inserted. At the Ringhals nuclear power plant in Sweden (Units 3 and 4), long-term exposure of fuel assemblies to excessive hold-down forces in the reactor led to accumulated deformation, causing the control rod to become stuck in the lower part of the fuel assembly and unable to be fully inserted [5].

Regarding the effect of fuel assembly bending on control rod drop behavior, Yue Ti et al. [6] used ABAQUS software and a multi-body dynamics analysis platform to calculate rod drop in straight, C-shaped, and S-shaped guide tube bends, providing a basis for determining the limit bending threshold for rod jamming caused by bending deformation. Liu Jiqiu et al. [7] employed the dynamic mesh technology of FLUENT software to calculate the rod drop of a new type of fuel control rod, analyzing the effects of

Check for updates

Academic Editor: Thomas Höhne

Received: 10 May 2026
Revised: 7 June 2026
Accepted: 12 June 2026
Published: 19 June 2026

Copyright: © 2026 by the authors. Licensee MDPI, Basel, Switzerland. This article is an open access article distributed under the terms and conditions of the Creative Commons Attribution (CC BY) license.

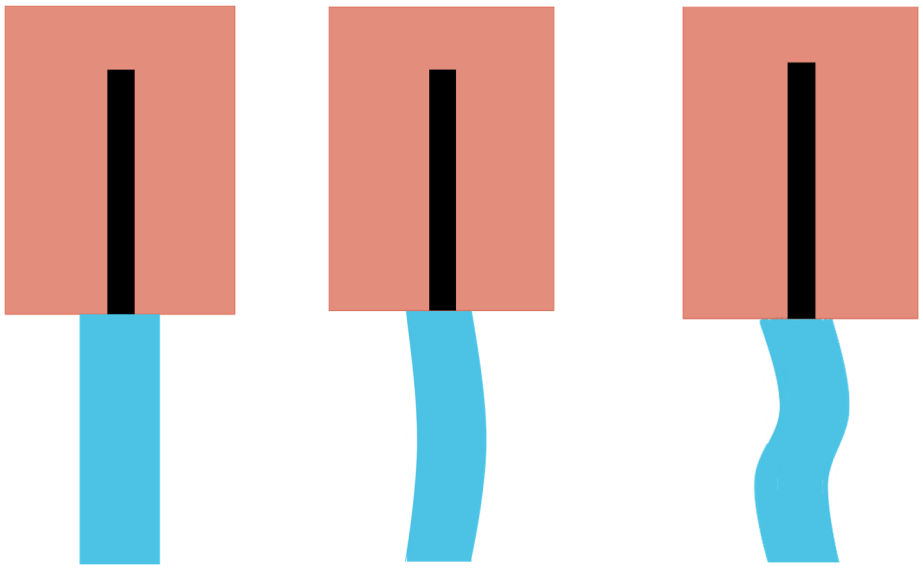
different rod diameters. Jun Liu et al. [8] used FLUENT dynamic mesh technology to study the effects of control rod misalignment and rod diameter variation on control rod drop behavior. Emmanuel Maurice Arthur et al. [9] investigated the dynamic characteristics of control rod drop in a lead-based research reactor using mathematical methods, establishing nonlinear differential equation systems for control rod motion and lead-bismuth flow to capture the influence patterns of key parameters. Comparison with experimental data from the existing literature demonstrated that the program has good applicability and reliability. In addition, Emmanuel Maurice Arthur et al. [10] also used CFD (CFX software) to model and analyze the control rod drop process in a lead-based research reactor, and the results indicated that the CFD model possesses good applicability and reliability. Ke Zhao et al. [11] studied the drop of control rods in a floating nuclear power plant under marine environmental conditions. They established the control rod motion equation and the Navier–Stokes equations, and validated the correctness of the model and algorithm through experiments. They analyzed the safety of control rod drop under normal and extreme marine conditions, and the results showed that the control rod drop remains safe under both conditions. Kim, J. Y. et al. [12] proposed a numerical analysis method based on computational fluid dynamics for control rod assemblies with complex geometries in sodium-cooled fast reactors, aiming to accurately predict the drop time and impact velocity during emergency shutdown. Building on this work, Son et al. [13] validated the effects of design modifications on the drop performance of control rods in sodium-cooled fast reactors through full-scale experiments. By increasing the weight of the control rod assembly from 48 kg to 57 kg, key indicators such as the rod drop time were significantly improved compared to the initial design. Dae-Guen Lim [14] proposed a neural network (DeepONet)-based model for real-time prediction of control rod drop motion. Validation results showed that the DeepONet predictions were in excellent agreement with the dynamic model, achieving displacement prediction accuracy of 99.39% and velocity prediction accuracy of 98.72% under different fuel assembly deformation conditions. Feng Wu et al. [15] employed statistical methods to analyze uncertainties in the control rod drop process, calculating the mean and standard deviation of response quantities such as rod drop time for two different types of reactors, and based on this, obtained the control rod drop response intervals and their corresponding probabilities. In terms of the moving mesh CFD method, Cheng-Hau Yang et al. [16] proposed a computational framework that integrates octree-based adaptive mesh refinement with the shifted boundary method for simulations of incompressible flow and fluid–thermal coupling. This approach uses vorticity magnitude to drive hierarchical dynamic mesh refinement, enabling the capture of complex vortical structures and sharp thermal gradients while significantly reducing computational costs compared to traditional uniform refinement methods.

Existing studies have primarily focused on control rod drop in new reactor types, while few investigations have addressed the effect of channel bending on control rod drop, especially the influence of flow field variations caused by channel bending; therefore, this paper uses the dynamic mesh technology of FLUENT software, to study the effect of C-shaped and S-shaped channel bends on rod drop time when the control rod descends without contacting the channel, with a focus on the influence of flow field changes caused by channel bending on control rod drop. The variations in rod drop time, rod drop velocity, static pressure on the control rod, and dynamic pressure are analyzed for different fluid media and different control rod masses.

2. Theoretical Model of Control Rod Drop

2.1. Force Analysis

The control rod drop models are shown in Figure 1, which depict a straight channel, a C-shaped bent channel, and an S-shaped bent channel, respectively. In the figure, the black area represents the control rod, the orange area represents the air domain, and the blue area represents the liquid domain. The model dimensions are listed in Table 1. During the drop process, the control rod does not come into contact with the channel and remains in vertical descent. The degree of channel bending is 90% of the clearance between the control rod and the channel, corresponding to a transverse bending displacement of 22.5 mm.



(**a**) Straight channel (**b**) C-shaped curved channel (**c**) S-shaped curved channel

Figure 1. Control rod drop model diagram.

Table 1. Control Rod Drop Model Dimensions.

Control Rod Diameter/mm	Control Rod Length/mm	Channel Inner Diameter/mm	Initial Height of Control Rod Bottom Surface/mm
50	1650	100	1250

During the control rod drop process, it is subjected to gravity, buoyancy, differential pressure force, and friction. Among these, gravity acts vertically downward, while the other forces act upward. The kinematic quantities of the control rod drop—such as acceleration and velocity—can be calculated using Newton's second law, as shown in Equations (1)–(5). The symbols in bold are vectors, and the positive direction is vertically downward.

$$F = G - F_B - F_P - F_f = ma \tag{1}$$

$$G = mg \tag{2}$$

$$F_B = \rho g V \tag{3}$$

$$F_P = \Delta P \cdot A \tag{4}$$

$$F_f = \frac{1}{2} \cdot k \cdot \rho \left(v_{rod} + v_{fluid} \right)^2 \cdot A \tag{5}$$

where F—resultant force on the control rod, N; G—gravity acting on the control rod, N; F_B—buoyancy acting on the control rod, N; F_P—differential pressure lift force acting on

the control rod, N; F_f—fluid friction force on the control rod during dropping, N; m—mass of the control rod, kg; a—acceleration of the control rod during dropping, m/s^2; g—gravitational acceleration, m/s^2; ρ—fluid density, kg/m^3; V—volume of fluid displaced by the control rod during dropping, m^3; ΔP—pressure difference between the top and bottom of the control rod, Pa; A—projected area of the control rod in the vertical direction, m^2; k—friction coefficient of the control rod; v—dropping velocity of the control rod, m/s; v_f—fluid velocity, m/s.

2.2. Dynamic Analysis

By combining the force analysis and dynamic analysis of control rod drop, the theoretical formula for the drop time can be derived, as detailed in Equations (6)–(9).

$$v_{rod}^2 - v_{rod_0}^2 = 2aS \rightarrow v_{rod}^2 = 2aS \tag{6}$$

$$f = \frac{1}{2} C\rho A v_{rod}^2 = C\rho A \cdot aS \tag{7}$$

$$mg - f = ma \rightarrow a = g - \frac{f}{m} = g - \frac{C\rho A \cdot aS}{m} \rightarrow a = \frac{g}{\left(1 + \frac{C\rho AS}{m}\right)} \tag{8}$$

$$S = \frac{1}{2} at^2 \rightarrow t = \sqrt{\frac{2S}{a}} = \sqrt{\frac{2S\left(1 + \frac{C\rho AS}{m}\right)}{g}} \tag{9}$$

where v_0—initial drop velocity of the control rod, 0; S—drop displacement of the control rod, m; f—fluid resistance, N; C—fluid resistance coefficient, which depends on the windward area, smoothness, and shape of the object; t—drop time of the control rod, s.

3. CFD Calculation Settings

The control rod drop model is meshed with hexahedral elements, and only the fluid domain is meshed. The mesh size is 4 mm, which is the same as that in Reference [8]. The fluid domain is divided into two regions based on mesh motion: a mesh motion region and a mesh stationary region. The meshes of the two regions are generated independently.

3.1. Description of the Calculation Example

The control rod drop calculation is divided into straight channel, C-shaped curved channel, and S-shaped curved channel. Based on the control rod mass and liquid medium type, a total of nine cases are classified, as summarized in Table 2. The control rod mass is consistent with that in Reference [8].

Table 2. Calculation case of control rod drop.

	Liquid Medium	Straight Channel	C-Shaped Curved Channel	S-Shaped Curved Channel
Control Rod Mass: 3.8 kg	Water	Case 1	Case 2	Case 3
Control Rod Mass: 24.5 kg	Water	Case 4	Case 5	Case 6
	Lead-Bismuth	Case 7	Case 8	Case 9

3.2. Dynamic Mesh Setting

The dynamic mesh method can adjust the internal grid nodes when the mesh deforms. It can be classified into the Layering method, Smoothing method, Remeshing method, and Overset method [17], as summarized in Table 3. The principle of the Layering method is as

follows: grids that are affected by boundary movement or undergo motion themselves are automatically merged or split when stretched or compressed to a certain size. The mesh changes by adding or removing layers one by one, with the mesh size remaining constant while the number of grid cells increases or decreases. The principle of the Smoothing method is as follows: the mesh connectivity within the computational domain is treated as spring connections. When the boundary movement causes the mesh to be stretched or compressed, the grid nodes move, the total number of grids remains unchanged, and the grid shape changes. The principle of the Remeshing method is as follows: when the mesh size and skewness exceed the maximum tolerable range, the mesh is reconstructed. This method is typically used in conjunction with the Smoothing method. The principle of the Overset method is as follows: coupling is achieved by exchanging data between receptor grid cells in one region and donor grid cells in another region.

Table 3. Overview of dynamic mesh methods [18].

	Layering	**Smoothing**	**Remeshing**	**Overset**
Applicable Scenarios	Unidirectional rigid body motion	Small deformation motion	Typically used with Smoothing, suitable for large deformation motion	Rigid body motion
Mesh Requirements	Structured mesh, relatively difficult to generate	Tetrahedral mesh, relatively easy to generate	Tetrahedral mesh, relatively easy to generate	Applicable to all mesh types, relatively easy to generate
Computational Performance	Relatively fast computation	Relatively slow computation	Relatively slow computation	Relatively slow computation

The control rod drop is a rigid-body motion. This paper simulates only the vertical motion of the control rod. To reduce computational time, the Layering method is selected for the simulation. To ensure more stable and reliable calculations, a combination of bottom layering and top layering is used to cause changes in the bottom and top meshes of the model, replacing the active deformation of the control rod mesh.

3.3. Boundary Conditions and Solver Settings

The initial position of the control rod drop is such that the bottom surface of the rod is just in contact with the liquid surface, and the entire control rod is in an air environment. The boundary conditions and solver settings are shown in Table 4.

Table 4. Boundary Conditions and Solver Settings.

	0.1 Mpa, 20 °C
Outlet Boundary of the Air Domain	pressure outlet
Initial Velocity of the Control Rod	0
Solver Model	Multiphase flow, K-e turbulence model
Dynamic Mesh Setting	Layering, 6 DOF
Time Step Size/s	0.0016–0.0080

4. Results and Discussion

The control rod drop time under the conditions of a straight channel, a control rod mass of 3.8 kg, and a water medium was used as the validation case. The drop time

calculated in this simulation is 0.64 s, compared to 0.67 s in reference [8], yielding a relative deviation of −4.5%.

4.1. Rod Drop Characteristics in the Straight Channel

Figure 2 shows the variation curves of drop time with displacement in the straight channel. The control rod with a mass of 24.5 kg in the water medium has the shortest drop time (0.52 s), followed by the control rod with a mass of 3.8 kg in the water medium (0.64 s), and the control rod with a mass of 24.5 kg in the lead-bismuth medium (0.74 s). Under the same medium, the drop time depends on the mass: the greater the mass, the shorter the drop time. Under different media, for the same mass, the drop time depends on the medium density: the greater the density, the longer the drop time, as shown in the dynamic Formulas (6)–(9) in Section 2.2.

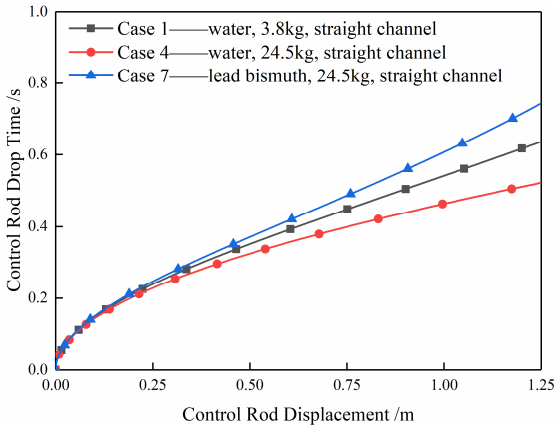


Figure 2. Variation Curve of Drop Time with Displacement.

From the above analysis, it can be seen that the control rod with a mass of 24.5 kg in the water medium has the fastest drop velocity, followed by the control rod with a mass of 3.8 kg in the water medium, and the control rod with a mass of 24.5 kg in the lead-bismuth medium. Figure 3 shows the curves of control rod drop velocity versus displacement. Under the same water medium, the greater the mass of the control rod, the faster the velocity increases, i.e., the greater the acceleration. For the same control rod, the greater the medium density, the slower the velocity increases, i.e., the smaller the acceleration, which can be derived from the acceleration calculation formula in Equation (8).

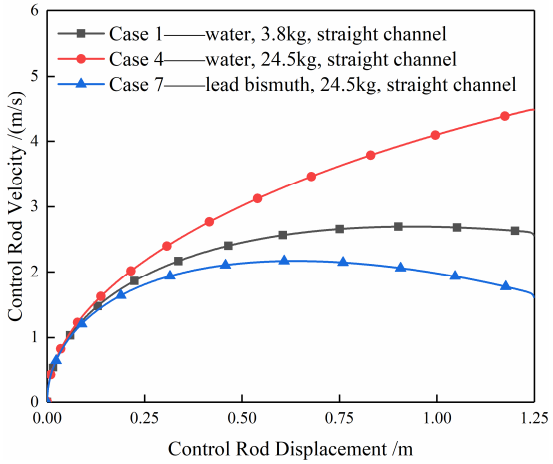


Figure 3. Variation Curve of Control Rod Drop Velocity with Displacement.

Figure 4 shows the curves of the overall average static pressure of the control rod versus displacement. The static pressure at the initial position is 0. As the drop displacement of the control rod increases, the static pressure gradually increases. However, the rate of increase in static pressure for the control rod in the lead-bismuth medium is much greater than that in the water medium. Under the same medium, the static pressures for different control rods are nearly equal, while under different media, the static pressures for the same control rod differ significantly. According to fluid statics, static pressure is positively correlated with the fluid medium density and the immersion depth, and is independent of the mass of the object.

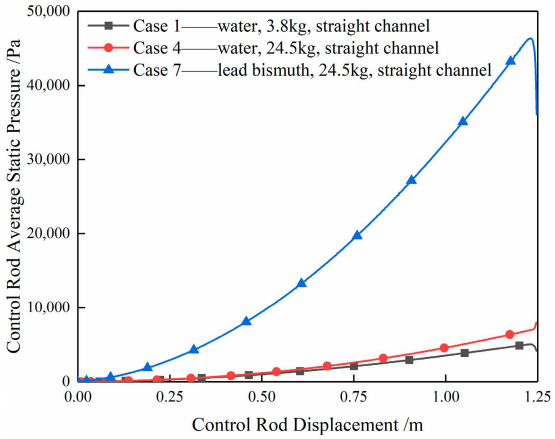


Figure 4. Variation Curve of Control Rod Overall Average Static Pressure with Displacement.

Figure 5 shows the curves of the overall average dynamic pressure of the control rod versus displacement. Dynamic pressure refers to the pressure generated by fluid flow. When the fluid flows at a certain velocity, its kinetic energy can be converted into pressure on the pipe wall or other obstacles. The calculation formula for dynamic pressure is given in Equation (10), where *v* is the fluid velocity. It can be seen from Figure 5 that in the water medium, the greater the mass of the control rod, the greater the dynamic pressure, because a larger control rod mass leads to a greater relative velocity between the fluid and the control rod, resulting in a larger dynamic pressure. For the same control rod, the dynamic pressure in the lead-bismuth medium is greater than that in the water medium. Although in the middle and late stages of the control rod drop, the drop velocity of the 24.5 kg control rod in the water medium is nearly 100% higher than that of the 24.5 kg control rod in the lead-bismuth medium, the density of the lead-bismuth medium is nearly 10 times that of the water medium, so the dynamic pressure in the lead-bismuth medium remains larger. However, this trend weakens in the final stage of the control rod drop.

$$P_{dynamic} = \frac{1}{2}\rho v^2 \tag{10}$$

4.2. Flow Field Changes Caused by the Curved Channel

Figure 6 shows the two-phase contour maps at the bottom for the straight, C-shaped curved, and S-shaped curved channels with a 3.8 kg control rod in the water medium. Liquid overflow occurs at the two-phase interface, but the overflow height does not exceed the top surface of the control rod. The overflow on both sides of the straight channel is symmetrically distributed, while differences in overflow height exist between the two sides of the C-shaped curved and S-shaped curved channels. Figure 7 shows the corresponding front-view velocity contour maps at the bottom. The liquid velocity distribution in the straight channel is relatively uniform within the channel, whereas the velocity distribu-

tion in the curved channels is uneven, and the complex curvature further increases the unevenness of the velocity distribution. Figure 8 shows the top-view velocity contour maps at one-quarter rod height after bottoming. The liquid velocity distribution is uneven in all three channels, but the straight channel exhibits a symmetrical distribution. In the C-shaped curved channel, the velocity in the narrow section is lower than that in the wide section, while in the S-shaped curved channel, the velocities in the two sections are comparable, but the velocity at the junction between the two sections decreases significantly. Figures 9 and 10 show the top-view velocity contour maps at two-quarters and three-quarters rod heights, respectively, both revealing symmetrical velocity distribution in the straight channel and uneven velocity distribution in the curved channels. In summary, the curvature of the channel leads to an uneven flow field distribution.

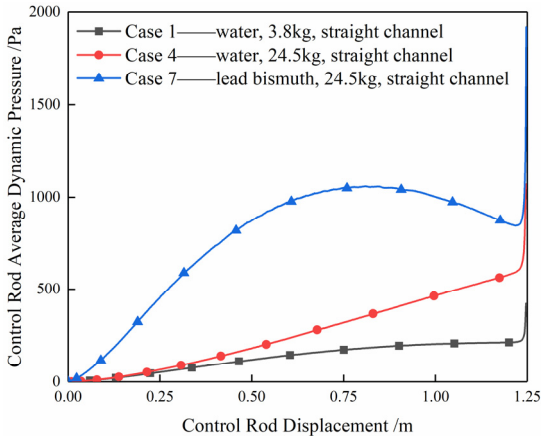


Figure 5. Variation Curve of Control Rod Overall Average Dynamic Pressure with Displacement.

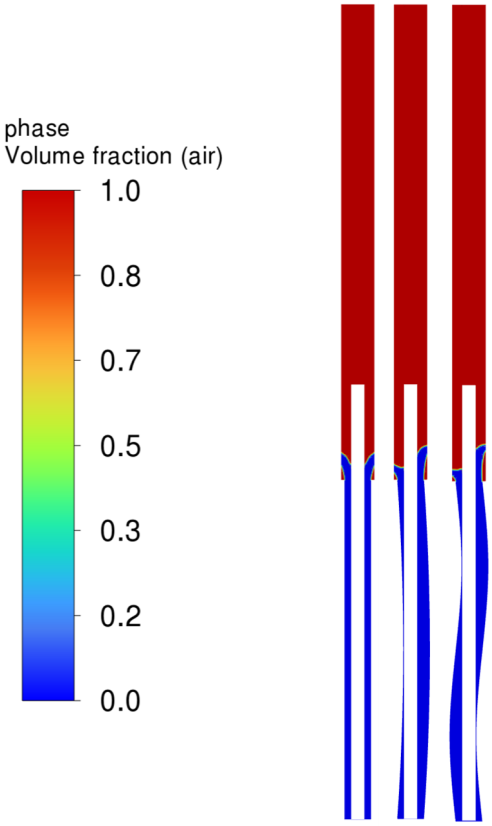


Figure 6. Two-Phase Contour Maps of the Control Rod at Bottoming for the Three Channels.

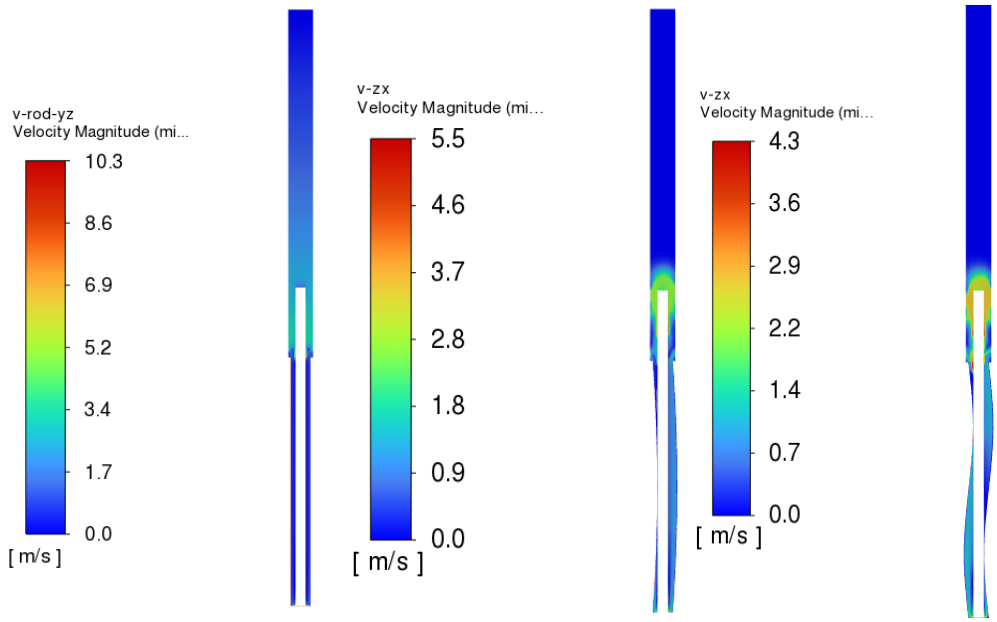
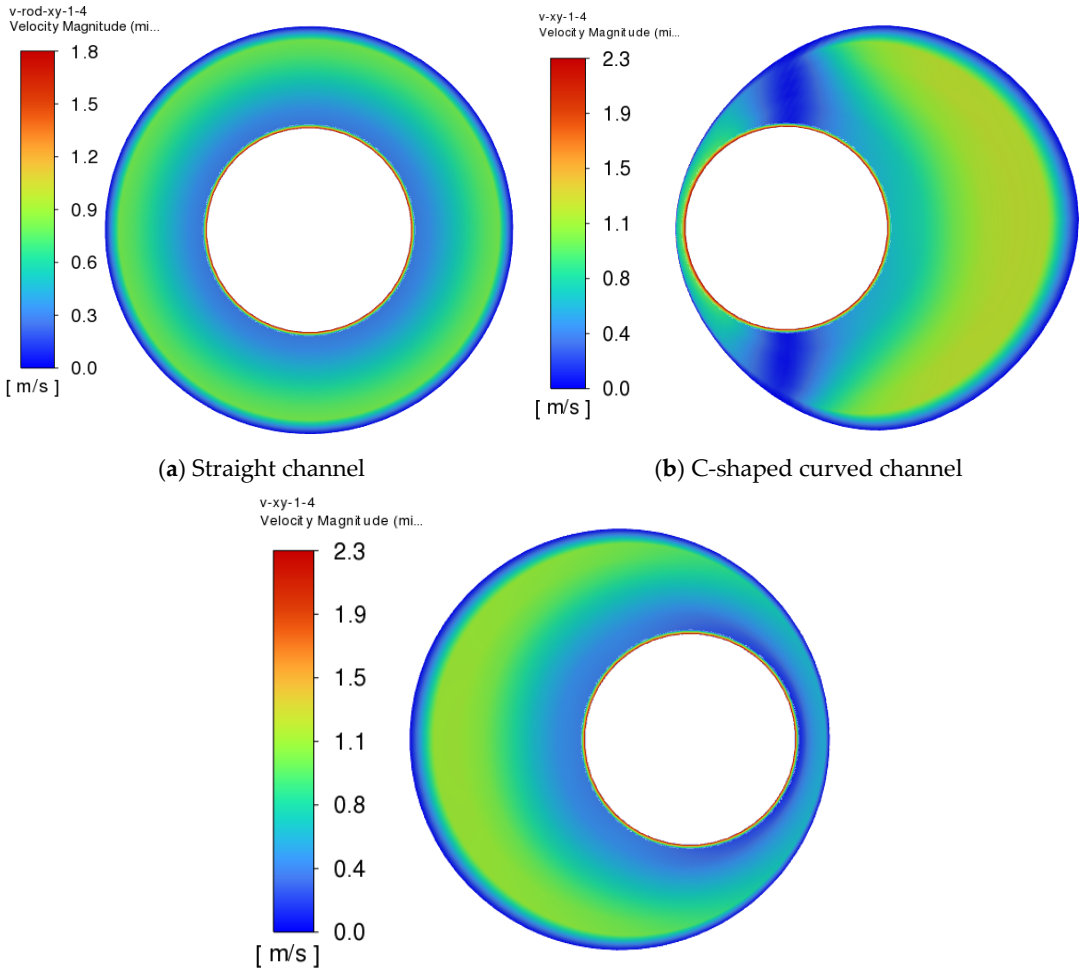


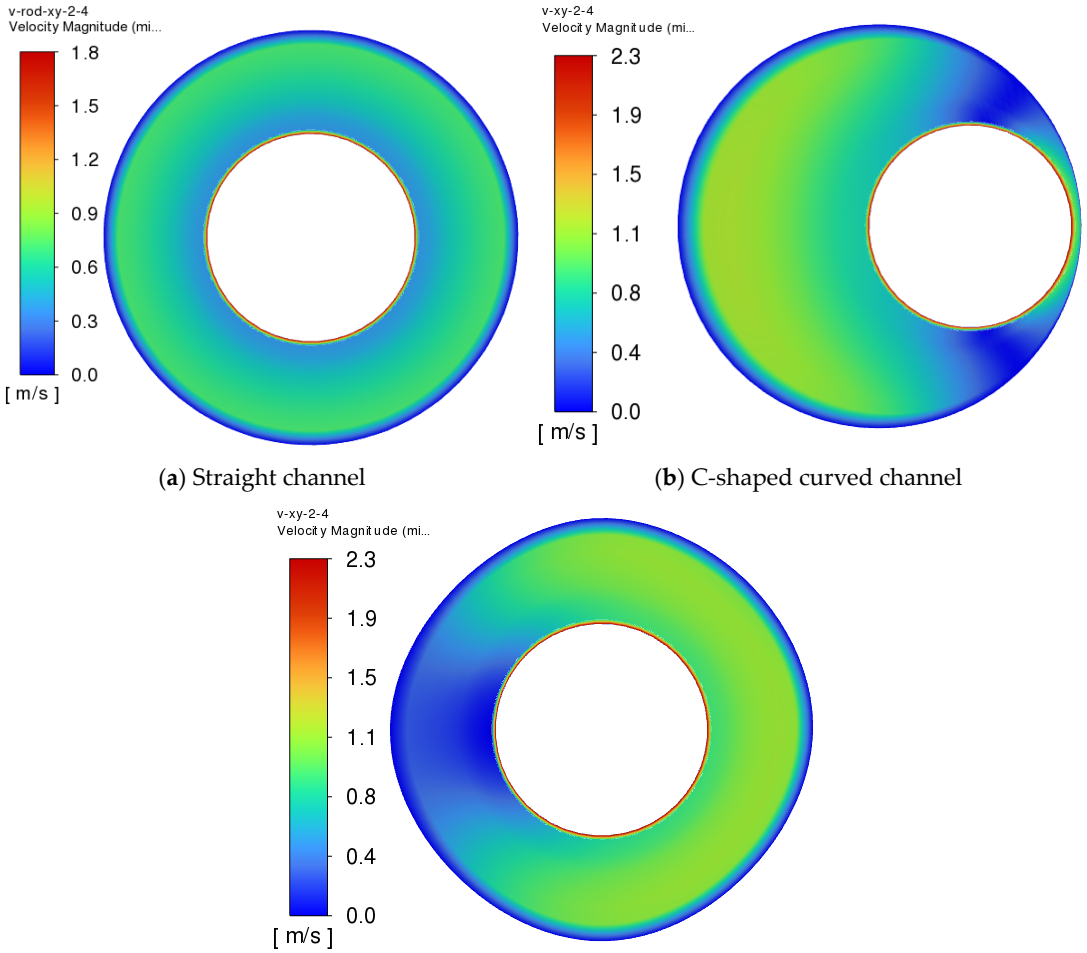
Figure 7. Front-View Velocity Contour Maps of the Control Rod at Bottoming for the Three Channels.



(**a**) Straight channel (**b**) C-shaped curved channel

(**c**) S-shaped curved channel

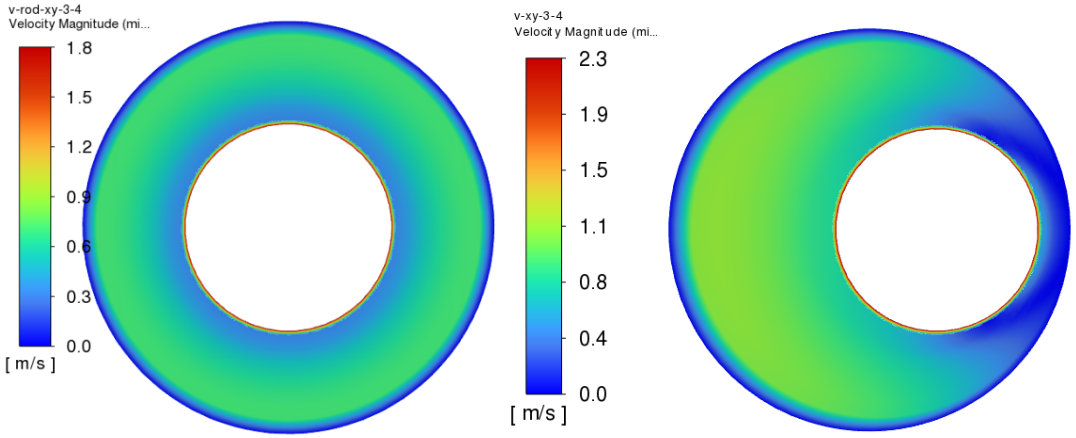
Figure 8. Top-View Velocity Contour Maps at One-Quarter Rod Height of the Control Rod at Bottoming for the Three Channels.



(**a**) Straight channel (**b**) C-shaped curved channel

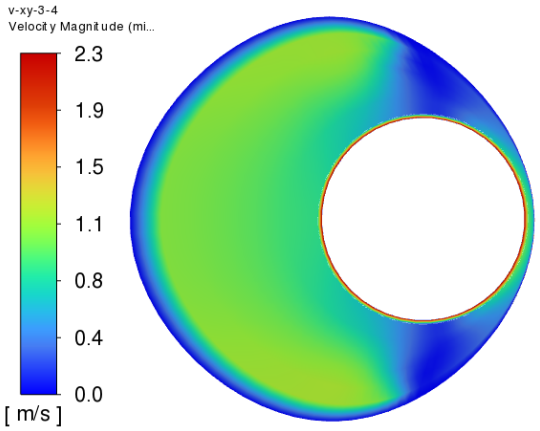
(**c**) S-shaped curved channel

Figure 9. Top-View Velocity Contour Maps at Two-Quarters Rod Height of the Control Rod at Bottoming for the Three Channels.



(**a**) Straight channel (**b**) C-shaped curved channel

Figure 10. *Cont.*



(**c**) S-shaped curved channel

Figure 10. Top-View Velocity Contour Maps at Three-Quarters Rod Height of the Control Rod at Bottoming for the Three Channels.

4.3. Effect of Channel Curvature on Control Rod Drop

Figures 11–13 show the curves of drop time versus displacement for different media and different control rods in curved channels. Figure 11 presents the drop time–displacement curves for a 3.8 kg control rod in a water medium. It can be seen from the figure that the drop curves of the control rod in the C-shaped curved and S-shaped curved channels coincide with that in the straight channel. For the same water medium, the drop curves of the 24.5 kg control rod also coincide among the three channels (see Figure 12). When the medium is changed to lead-bismuth, the drop curves of the 24.5 kg control rod still coincide among the three channels (see Figure 13). The above indicates that when the control rod does not contact the channel, the effect of flow field changes caused solely by channel curvature on the control rod drop is negligible.

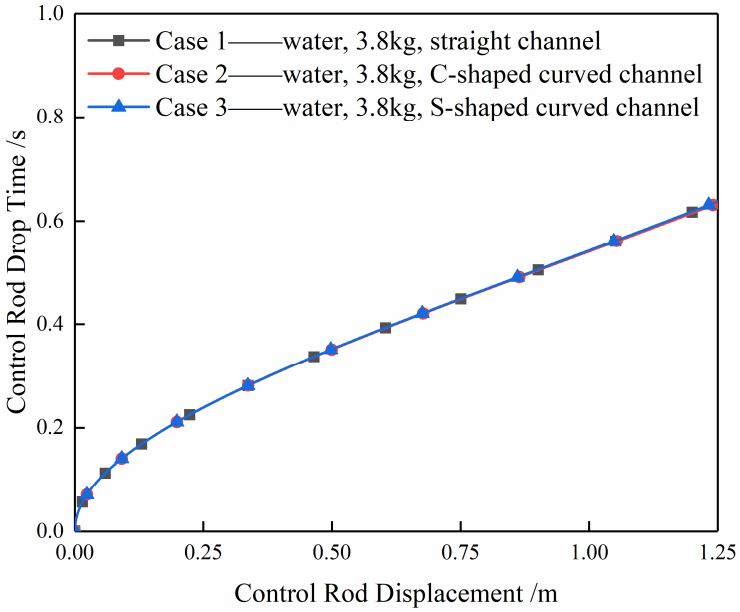


Figure 11. Variation in Control Rod Drop Time with Displacement for a 3.8 kg Control Rod in Water Medium under Channel Curvature.

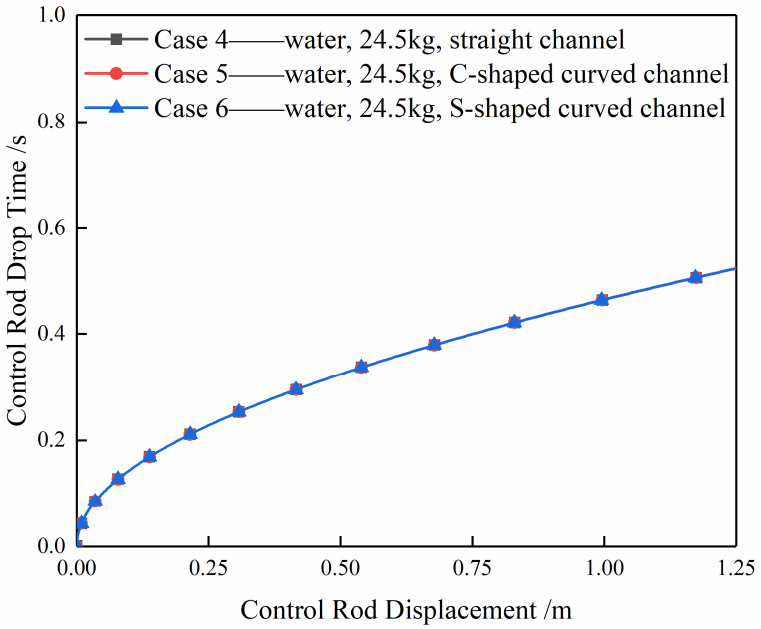


Figure 12. Variation in Control Rod Drop Time with Displacement for a 24.5 kg Control Rod in Water Medium under Channel Curvature.

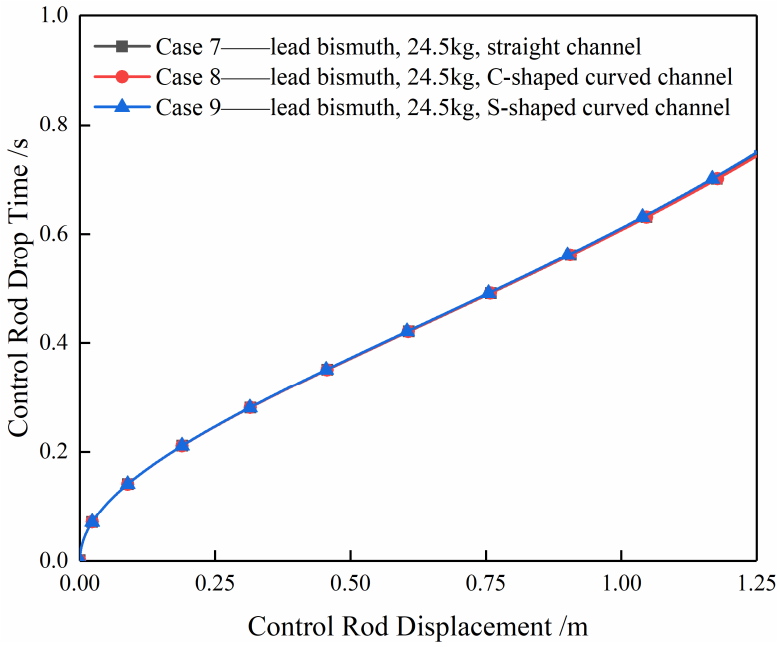


Figure 13. Variation in Control Rod Drop Time with Displacement for a 24.5 kg Control Rod in Lead-Bismuth Medium under Channel Curvature.

5. Conclusions

This paper analyzes the characteristics of drop time, velocity, static pressure, and dynamic pressure of the control rod under different media and different control rod masses in a straight channel, and further compares the drop time among the C-shaped curved, S-shaped curved, and straight channels. The following conclusions are drawn:

(1) Under the same medium, the greater the mass of the control rod, the shorter the drop time. The type of liquid medium has a significant effect on the drop time. For a 24.5 kg control rod in a straight channel, the drop time in the lead-bismuth medium is 42% longer than that in the water medium.

(2) The static pressure of the control rod is related to the liquid medium and immersion depth, but is independent of the control rod mass. The dynamic pressure of the control rod is related to the liquid medium and drop velocity (control rod mass).
(3) For the C-shaped curved and S-shaped curved channels where the control rod does not contact the channel during dropping, the flow field variation does not affect the drop time.

Author Contributions: Conceptualization, S.Z. Formal analysis, S.Z. Methodology, S.Z. Resources, Q.L. Writing—original draft preparation, S.Z. Writing—review & editing, C.W., Y.T., Y.M., and J.T. All authors have read and agreed to the published version of the manuscript.

Funding: This research received no external funding.

Institutional Review Board Statement: Not applicable.

Informed Consent Statement: Not applicable.

Data Availability Statement: Data will be made available on request.

Conflicts of Interest: Authors Siyu Zou, Chang'e Wu, Yangyang Tang, Qifeng Lv, Yue Ma and Jinghua Tang were employed by the China Nuclear Power Technology Research Institute. The authors declare that the research was conducted in the absence of any commercial or financial relationships that could be construed as a potential conflict of interest.

References

1. Rudling, P.; Adamson, R.B. Performance and inspection of zirconium alloy fuel bundle components inlight water reactors (LWRs). In *Matreials Ageing and Degradation in Light Water Reactors*; Woodhead Publishing: Sawston, UK, 2013; pp. 246–283.
2. Wanninger, A.; Seidl, M.; Macian-Juan, R. Mechanical analysis of the bow dormation of a row of fuel assemblies in a PWR core. *Nucl. Eng. Technol.* **2018**, *50*, 297–305. [CrossRef]
3. Andersson, T.; Almberger, J.; Björnkvist, L. A Decade of AssemblyBow Management at Ringhals. In Proceedings of the Structural Behaviour of Fuel Assemblies for Water Cooled Reactors, Cadarache, France, 2–26 November 2004; pp. 129–136.
4. Li, W.; Xiao, Z. Bending Deformation Mechanism and Avoidance Measures of PWR Fuel Assembly. *Nucl. Power Eng.* **2008**, *29*, 55–57+73.
5. Jacobson, S.; Francillon, E. Incomplete Control Rod Insertion due to Extreme Fuel Element Bow. In *Proceedings of the Specialist Meeting on Nuclear Fuel and Control Rods: Operating Experience, Design Evolution and Safety Aspects*; Nuclear Energy Agency: Paris, France, 1997; pp. 265–271.
6. Yue, T.; Zheng, L.; Zhu, F.; Wang, H.Y.; Yuan, P.; Sun, Y.; Deng, S. Analysis of Rod Drop Behavior in Deformed Channel of Improved Control Rod Assembly Based on Rigid-Flexible Coupling. *Nucl. Power Eng.* **2022**, *43*, 129–134.
7. Liu, J.; He, X.; Dai, J.; Wu, Q.; Hao, S.J. Prediction of Cold-State Rod Drop Behavior Characteristics of Fuel Control Rod Based on Fluent. *Nucl. Power Eng.* **2025**, *46*, 109–114.
8. Liu, J.; He, L.; Peng, Q.; Chen, X.; Liu, X.; Wei, Y. Eccentric drop of a control rod in the guide tube with annular gap flow. *Nucl. Eng. Des.* **2023**, *415*, 112744. [CrossRef]
9. Arthur, E.M.; Zhang, C.; Debrah, S.K.; Yamoah, S.; Wang, L. Analysis of the drop dynamics of control rod assembly in a LBE-cooled research reactor. *Ann. Nucl. Energy* **2020**, *149*, 107778. [CrossRef]
10. Arthur, E.M.; Zhang, C.; Debrah, S.K.; Yamoah, S.; Wang, L. Numerical simulation for the control rod assembly drop time evaluation in a LFR. *Heliyon* **2022**, *8*, e11540. [CrossRef] [PubMed]
11. Zhao, K.; Wu, F.; Ai, C.; Chen, C.; Wu, X.; Zhong, P.; Yan, J. Modeling and analysis of control rod drop in a floating nuclear power plant under ocean conditions. *Ocean Eng.* **2025**, *338*, 121992. [CrossRef]
12. Kim, J.Y.; Yoon, K.; Oh, S.H.; Ko, S. CFD Analysis to Estimate Drop Time and Impact Velocity of a Control Rod Assembly in the Sodium Cooled Fast Reactor. *J. Fluid Mach.* **2015**, *18*, 5–11. [CrossRef]
13. Son, J.G.; Lee, J.H.; Kim, H.W.; Kim, S.K.; Kim, J.B. Influence of Design Modification of Control Rod Assembly for Prototype Generation IV Sodium-cooled Fast Reactor on Drop Performance. *Nucl. Eng. Technol.* **2019**, *51*, 1926–1932. [CrossRef]
14. Lim, D.-G.; Lee, G.-Y.; Park, Y.-H. Application of DeepONet to predict transient drop motion of the control rod in real-time. *Nucl. Eng. Technol.* **2025**, *57*, 103620. [CrossRef]
15. Wu, F.; Zhao, K.; Zhao, L.; Chen, C.; Zhong, W. Uncertainty analysis of the control rod drop based on the adaptive collocation stochas-tic perturbation method. *Ann. Nucl. Energy* **2023**, *190*, 109873. [CrossRef]

16. Yang, C.-H.; Scovazzi, G.; Krishnamurthy, A.; Ganapathysubramanian, B. Octree-based adaptive mesh refinement and the shifted boundary method for efficient fluid dynamics simulations. *Adv. Comput. Sci. Eng.* **2025**, *4*, 57–84. [CrossRef]
17. Zhang, L.; Deng, X.; Zhang, H. Review of Dynamic Grid Generation Technology and Unsteady Computational Methods. *Adv. Mech.* **2010**, *40*, 424–447.
18. Zhou, H.; Zhong, K.; Jia, H.; Kang, Y. Analysis of the effects of dynamic mesh update method on simulating indoor airflow induced by moving objects. *Build. Environ.* **2022**, *212*, 108782. [CrossRef]

Disclaimer/Publisher's Note: The statements, opinions and data contained in all publications are solely those of the individual author(s) and contributor(s) and not of MDPI and/or the editor(s). MDPI and/or the editor(s) disclaim responsibility for any injury to people or property resulting from any ideas, methods, instructions or products referred to in the content.